Chemical Engineering Journal 322 (2017) 140–148

Contents lists available at ScienceDirect

Chemical Engineering Journal

journal homepage: www.elsevier.com/locate/cej

Mechanisms and control of single-step microfluidic generation of multi-core double emulsion droplets

Seyed Ali Nabavi [a,b], Goran T. Vladisavljević [a,*], Vasilije Manović [b,*]

[a] Department of Chemical Engineering, Loughborough University, Loughborough LE11 3TU, United Kingdom
[b] Combustion and CCS Centre, Cranfield University, Cranfield MK43 0AL, United Kingdom

HIGHLIGHTS

- The mechanisms of single-step formation of multi-core double emulsion were revealed.
- Phase diagrams for predicting number of encapsulated inner drops were mapped out.
- The jet pinch-off process was accompanied and affected by presence of a vortex flow.
- The formation regime of inner phase affected the number of encapsulated inner drops.
- Large single-core capsules were made from dual-core drops with unstable inner drops.

GRAPHICAL ABSTRACT

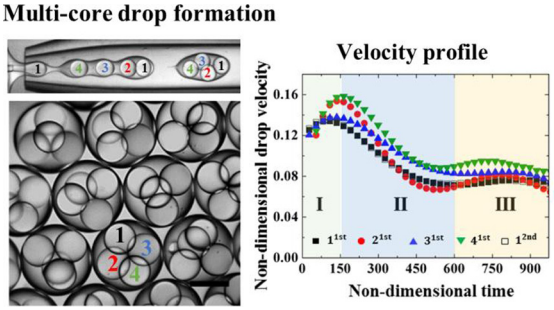

ARTICLE INFO

Article history:
Received 17 January 2017
Received in revised form 12 March 2017
Accepted 2 April 2017
Available online 4 April 2017

Keywords:
Multi-core double emulsion drops and capsules
Capillary microfluidics
Dripping-to-jetting transition
Droplet formation dynamics
Micro-particle image velocimetry
Core/shell silicon microcapsules

ABSTRACT

Single-step generation of monodisperse multi-core double emulsion drops in three-phase glass capillary microfluidic device was investigated using a micro-particle image velocimetry (micro-PIV) system. Phase diagrams were developed to predict the number of encapsulated inner drops as a function of the capillary numbers of inner, middle and outer fluid. The maximum stable number of inner drops cores in uniform double emulsion drops was six. Starting from core/shell drops, the formation of double emulsion drops with multiple cores was achieved by decreasing the capillary number of the outer fluid and increasing the capillary number of the middle fluid. A stable continuous jet of the middle fluid loaded with inner drops was formed at high capillary numbers of the middle fluid. Empirical correlations predicting the size and generation frequency of inner drops as a function of the capillary numbers and the device geometry were developed. Dual-core double emulsion drops were used as templates for the fabrication of polymeric capsules using "on-the-fly" photopolymerisation. The capsule morphology was controlled by manipulating the stability of the inner drops through adjusting the concentration of the lipophilic surfactant in the middle fluid. At low concentration of the lipophilic surfactant, inner drops coalesced during curing and single compartment capsules with thin shells were produced from dual-core drops. The core/shell capsules produced from multi-core drops were monodispersed and larger than those produced from core/shell drops in the same device.

* Corresponding authors.
E-mail addresses: g.vladisavljevic@lboro.ac.uk (G.T. Vladisavljević), v.manovic@cranfield.ac.uk (V. Manović).

http://dx.doi.org/10.1016/j.cej.2017.04.008
1385-8947/

1. Introduction

Multi-core double emulsions are complex emulsions composed of several inner drops dispersed in an immiscible middle phase, which is itself dispersed in the outer phase. They can be used for encapsulation of multiple reactive components for triggered reaction and mixing [1–3], co-culture of multiple cells in cell-based therapies [4], encapsulation and sequential release of incompatible active materials and liquids while avoiding cross-contamination [5], and the production of multi-compartment capsules [6]. Conventionally, multiple emulsions are produced in two consecutive emulsification steps through high-shear mixing of immiscible liquids [7]. However, this approach is associated with broad particle size distribution, low batch-to-batch reproducibility, low encapsulation efficiency, high energy consumption, and a lack of control over the size of the drops and the number of encapsulated inner drops [8,9].

Microfluidic emulsification is a promising tool for reproducible production of monodispersed multiple emulsion drops of versatile morphology [5,10–12]. Multi-core drops are usually produced using two consecutive T-junction [8,13], co-flow [10,11,14–16], and flow-focusing [17,18] drop makers. Perro et al. [16] used two consecutive co-flow makers made of fused silica capillaries to produce structured polymersomes and map out phase diagrams predicting the number of inner drops as a function of fluid flow rates. The number of inner drops decreased as the outer and middle phase flow rates increased. Okushima et al. [13] used two consecutive T-junctions made on a Pyrex glass to produce double emulsion drops with a controlled number of inner drops. The number of inner drops was found to increase with increasing flow rate of the inner phase. Using a two-step microfluidic device composed of three coaxial glass capillaries, Kim et al. [11] observed that the number of inner drops increased with increasing middle-to-inner volumetric flow rate ratio. Chu et al. [10] derived an empirical equation to predict the number of inner drops in multi-core droplets produced in a glass capillary device consisting of two consecutive co-flow drop makers. The number of inner drops was reduced by increasing the outer phase flow rate.

In the two-step emulsification approach, the generation of inner and outer drops is spatially separated; thus, synchronising the frequency of drop generation at different steps requires delicate control of individual flow rates [5]. Single-step microfluidic emulsification methods [6,19,20], e.g., a combined co-flow and counter-current flow focusing (Fig. 1a) [21], in a three-phase glass capillary device, can overcome this disadvantage, since the flow rates of the inner and middle fluid do not need to be synchronised. Moreover, one-step processes are advantageous for very thin-shelled core/shell drops, which are difficult to create in a two-step process. In addition, the capillary device for single-step emulsification is easier to fabricate than the device composed of two sequential drop generation units [10,15], due to simpler design and smaller number of capillaries and connectors [6,22].

Three main regimes of double emulsion generation in three-phase glass capillary devices are dripping, widening jetting, and narrowing jetting. In the dripping regime, highly uniform drops are formed near the orifice of the collection tube, while widening and narrowing jetting are associated with the production of polydispersed large and small drops, respectively, further downstream of the orifice [23,24]. For highly uniform multi-core drops, the cores should be formed in the dripping regime and the outer drops in the dripping-to-widening jetting transition regime [6]. Lee et al. [6] used a three-phase glass capillary to produce nonspherical colloidosomes. The higher inner and middle phase flow rates and the lower outer phase flow rates favoured encapsulation of larger numbers of inner drops. Although Lee et al. [6] briefly reported the effect of flow rates on the number of encapsulated inner drops, however, the mechanism of single-step formation of multi-core double emulsion drops has not yet been fully understood and needs to be investigated.

The purpose of this work is an in-depth investigation into the mechanisms of single-step generation of multiple emulsion drops in a co-flow/flow focusing microfluidic geometry. Novel phase diagrams have been developed to depict the effect of capillary numbers of the inner, middle, and outer fluids on the number of inner drops, and determine the operating conditions for successful production of double emulsions. The flow field during jet pinch-off was visualised by seeding charged latex beads in the outer phase. The generated drops were used as templates to produce capsules with controlled number of compartments via "on-the-fly" photopolymerisation. The number of cores in the capsule was controlled by manipulating the stability of inner drops during curing by varying the concentration of lipophilic surfactant in the middle

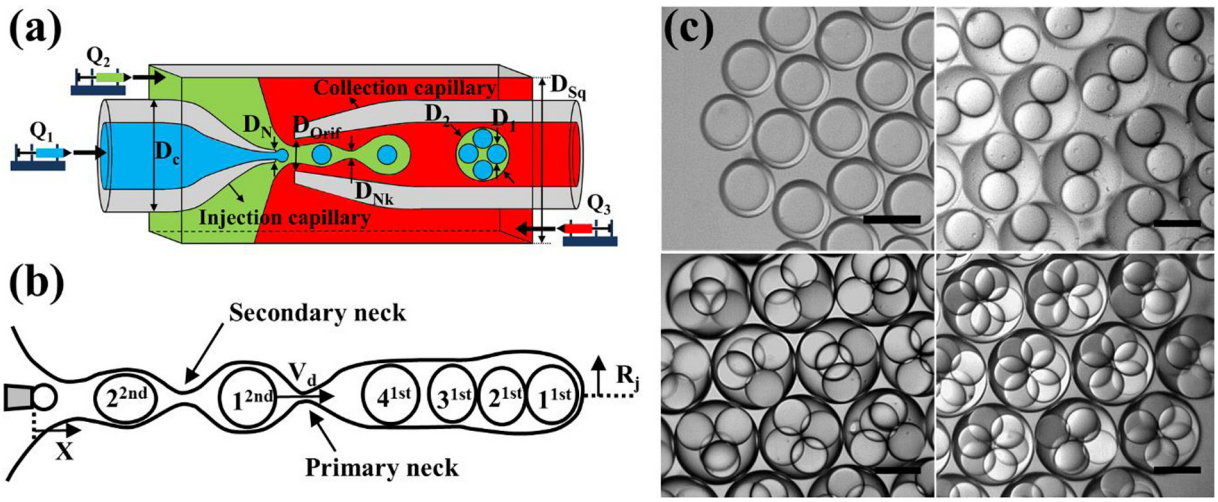

Fig. 1. (a) A schematic of the microfluidic device used in this work: Q_1, Q_2, Q_3 = flow rates of inner, middle and outer phase, D_1, D_2 = diameters of inner and outer drop, D_{sq} = inner width of square capillary, D_c = outer diameter of the injection tube, D_N, D_{orif} = orifice diameters of the injection and collection tube, D_{Nk} = neck diameter; (b) Schematic of a middle phase jet with the primary and secondary neck (V_d = velocity of the 1^{2nd} inner drop); (c) Optical images of the generated drops composed of one, two, four, and six inner drops. All scale bars are 500 μm.

phase. The microfluidic method developed in this work can be used for production of relatively large silicon rubber-based capsules for encapsulation of CO_2 absorbents [25,26].

2. Experimental procedure

2.1. Materials

K_2CO_3 and glycerol were supplied by Fisher Scientific (UK). Polyvinyl alcohol (PVA, M_w = 13,000–23,000 g mol^{-1}, 87–89% hydrolysed), Pluronic® F-127 (PF-127), 2 μm carboxylate-modified polystyrene latex beads, and *m*-cresol purple were purchased from Sigma-Aldrich, UK. Dow Corning® 749 Fluid (DC 749) was supplied by Univar (UK). Polydimethylsiloxane oil (Dow Corning 200 fluid, 20 CST) was obtained from VWR (UK). Octadecyltrimethoxysilane (OTMS) and 2-[methoxy(polyethyleneoxy)propyl]trimethoxysilane (TMS-PEG) were purchased from Fluorochem, Ltd. (UK). Semicosil® 949 UV A/B, a UV-curing silicone rubber was donated by Wacker Chemie (UK). The reverse osmosis water was supplied from a Milli-Q plus apparatus. The fluid densities, viscosities and interfacial tensions were measured using a pycnometer, capillary viscometer, and Krüss DSA-100 pendant drop tensiometer, respectively.

2.2. Droplet production

2.2.1. Fabrication of glass capillary device

A Flaming/Brown micropipette puller (P-97, Sutter Instrument Co.) was used to pull round glass capillaries (I.D. = 0.58 mm, O.D. = 1 mm, Intracel, UK) that were used as injection and collection tubes. The tips were polished to the desired orifice size using an abrasive paper (Black Ice Waterproof T402, Alpine Abrasives, UK) and inspected using a microforge microscope (Narishige MF-830, Japan). OTMS was used to make the injection orifice hydrophobic and TMS-PEG was used to enhance hydrophilic properties of the collection tube. The injection and collection capillaries were then inserted into a square glass capillary (inner width = 1.05 ± 0.1 mm, AIT Glass, Rockaway, US) from two opposite ends, placed at the desired distance from each other and axially aligned. The capillaries were fixed into position on a microscope slide using a 2-part 5-Minute Epoxy® glue (Devcon, UK). To introduce the three phases to the device, three hypodermic needles with polypropylene hubs (BD Precisionglide® 20 G, Sigma-Aldrich, UK) were attached to the capillaries and sealed with the epoxy glue. The device was left 4–5 h before use to ensure that the glue was fully cured.

2.2.2. Double emulsion formation

A schematic of the drop production process is shown in Fig. 1a. The fluids were delivered to the microfluidic device using Harvard Apparatus 11 Elite syringe pumps with gastight glass syringes (VWR Catalyst Company, UK), and polyethylene medical tubing (I.D. = 0.86 mm, O.D. = 1.52 mm, Fisher Scientific, UK). The drops were formed upon break-up of a coaxial jet composed of two co-flowing liquids in the collection tube (Fig. 1b).

2.3. Image analysis and particle tracking

An inverted microscope (XDS-3, GX Microscopes, UK) and Phantom V9.0 high-speed camera interfaced to a PC computer were used to observe and record the drop generation process. The time-dependent movements of inner drops were tracked by analysing successive frames captured with a resolution of 768 × 576 pixels at 2000 Hz with ImageJ software. The flow field was visualised using a micro-particle image velocimetry (microPIV) system incorporating 2 μm charged latex beads seeded in the outer fluid, a visible light source and the Matlab-based PIVlab (V 1.4) software. The minimum concentration of the tracer particles of 0.167 μg/mL and 20× objective lens were used to obtain acceptable visualisation outputs.

2.4. Dimensionless numbers

Non-dimensional numbers used in this study are the capillary numbers of the inner, Ca_1, middle, Ca_2 and outer phase, Ca_3, which are the ratio of viscous to interfacial tension forces, the Weber number for the inner phase, We_1, that gives the ratio of inertial to interfacial tension force in the inner phase, and the non-dimensional time, τ:

$$Ca_1 = \frac{\mu_1 V_{1,N}}{\sigma_{12}} \quad Ca_2 = \frac{\mu_2 V_2}{\sigma_{23}} \quad Ca_3 = \frac{\mu_3 V_3}{\sigma_{23}}$$

$$We_1 = \frac{\rho_1 V_{1,N}^2 D_N}{\sigma_{12}} \quad \tau = \frac{V_{1,N} t}{R_N}$$

where ρ, σ, μ, and V are the density, interfacial tension, dynamic viscosity and velocity, respectively (the subscripts 1, 2, and 3 stand for the inner, middle, and outer phase, respectively), R_N is the radius of the injection nozzle, and t is the time. The characteristic fluid velocities are:

$$V_{1,N} = 4Q_1/\left(\pi D_N^2\right)$$

$$V_2 = Q_2/\left(D_{sq}^2 - \pi D_c^2/4\right)$$

$$V_3 = Q_3/\left(D_{sq}^2 - \pi D_c^2/4\right)$$

3. Results and discussion

3.1. Formation of multiple emulsion drops with stable inner drops

Fig. 2a shows the temporal evolution of multiple emulsion drops consisting of 4 inner drops. The fluids are indicated in Table 1 and flow rates are defined in the caption to Fig. 2.

The first inner drop encapsulated in the outer drop will be referred to as the first (1^{1st}) drop (shown in red at τ = 0), and the subsequent inner drops will be denoted as the second (2^{1st}), third (3^{1st}), and fourth (4^{1st}) drop, respectively. The fifth drop (shown in red at τ = 612), will become the first inner drop encapsulated in the next outer drop and will be denoted as the 1^{2nd} drop. The primary neck formed downstream of the 1^{1st} drop (Fig. 1b) gets thinner and thinner until a pinch-off finally takes place. On the other hand, the secondary neck formed temporarily upstream of each inner drop disappears after reaching a certain minimum thickness.

The drop formation process can be divided into three main steps: (1) formation of inner drops by multiple break-ups of the inner fluid jet; (2) advection of inner drops through the middle fluid and their interaction with the growing perturbations on the outer interface; (3) break-up of the middle fluid jet and encapsulation of inner drops in the outer drop.

At τ = 0 (Fig. 2a), the primary neck of the previous outer drop has not yet collapsed and the 1^{1st} drop (shown in red) has just emerged. At τ = 95, the middle fluid thread of the previous drop has collapsed and the previous outer drop was detached. The 1^{1st} drop has an elongated shape, which is unstable because of the different radii of curvature across the interface, causing the drop velocity to increase (Fig. 2b). At τ = 136, the 1^{1st} drop was detached and reached the maximum velocity, after which it started to slow down due to rising capillary pressure in the thinning primary neck. The secondary neck of the 1^{1st} drop was formed at τ = 245 and reached the minimum thickness at τ = 259, after which it widened to allow the 2^{1st} drop to pass through and approach the 1^{1st} drop.

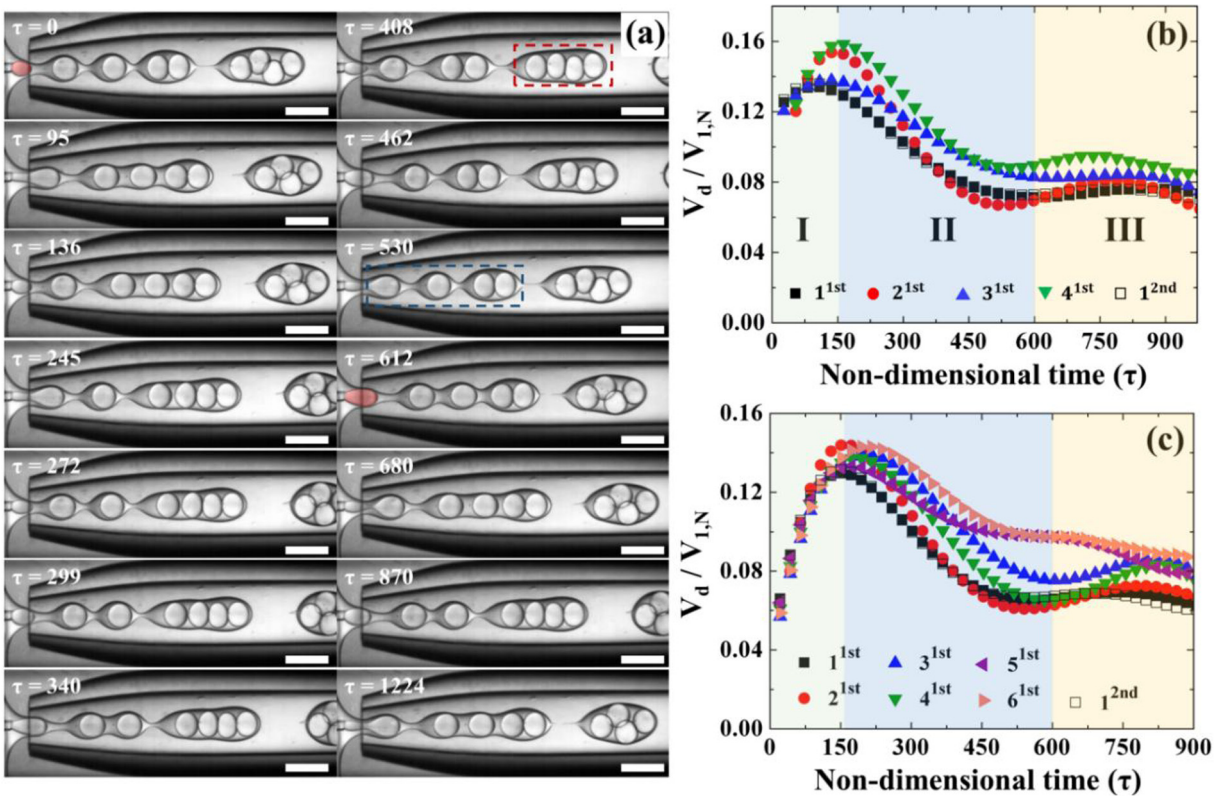

Fig. 2. (a) Image sequences for the formation of double emulsion drops with 4 inner drops. All scale bars are 400 μm; (b–c) The velocity of inner drops as a function of time during formation of multiple emulsion drops with: (b) four cores and (c) six cores. For (a) and (b): Q_1 = 2.4 mL/h, Q_2 = 2 mL/h, Q_3 = 12 mL/h, $V_{1,N}$ = 0.34 m/s, f_1 = 100 Hz, f_2 = 25 Hz. For (c): Q_1 = 2 mL/h, Q_2 = 1.2 mL/h, Q_3 = 6 mL/h, and $V_{1,N}$ = 0.27 m/s, f_1 = 71 Hz, f_2 = 12 Hz, where f_1 and f_2 are generation frequencies of inner and outer drops, respectively. The fluid properties are indicated in Table 1, D_{orif} = 327 μm, and D_N = 50 μm.

Table 1
The densities, ρ, the dynamic viscosities, μ, and the interfacial tensions, σ, for the fluids used in Fig. 2.

		ρ (kg/m^3)	μ (mPa·s)	σ* (mN/m)
Inner phase	85 wt% glycerol in Milli-Q water	1225	109	29.9
Middle phase	2 wt% DC 749 in Dow Corning 200 Fluid, 10 CST	940	10.4	31.8
Outer phase	70 wt% glycerol + 2 wt% PVA in Milli-Q water	1118	33	

* The interfacial tension was measured in the absence of stabilisers.

Due to decay of the secondary neck, the maximum velocity of the 2^{1st} drop was higher than that of the 1^{1st} drop (Fig. 2b). At τ = 408, the 3^{1st} drop was pinched off but the maximum velocity reached by that drop was lower than the maximum velocity of the 2^{1st} drop because the pinch-off process of the primary outer drop (marked by the red dashed rectangle) entered its final stage characterised by a high pressure in the neck. At τ = 612, the 4^{1st} drop was pinched off and reached higher velocity than the previous inner drops, because the outer drop was detached at τ ≈ 600 causing the middle phase jet to accelerate afterwards (Fig. 2b). The subsequent outer drop in the blue dashed rectangle was pinched off at τ = 1224.

Fig. 2b shows the temporal variations of the velocity of inner drops in dimensionless coordinates for the image sequences shown in Fig. 1. For easier comparison, the formation of each inner drop starts at τ = 0. Region I (τ < 150) was characterised by an increase in the velocity of inner drops and corresponds to the growth and pinch-off of each inner drop. During this step, the drop shape increasingly deviates from spherical due to increasing drag force acting from the middle fluid. Thus, the forming drop is increasingly unstable, since the difference in Laplace pressure between the upstream face of the drop and its neck increases, which causes the velocity to rise. The maximum relative velocity ($V_d/V_{1,N}$) for the 2^{1st}, 3^{1st}, and 4^{1st} drop of 0.15, 0.14, and 0.16, respectively, was achieved later in the cycle and was greater than the maximum relative velocity for the 1^{1st} drop of 0.13. The low velocity of the 1^{1st} drop was due to thinning of the primary neck, which prevented further advection of the 1^{1st} drop through the middle phase.

Region II (150 < τ < 600) corresponds to the decrease in the velocity of inner drops, which can be attributed to the break-up process of the primary outer drop, associated with rising pressure in the primary neck. Region III (τ > 600) occurs after pinch-off of the primary outer drop and is characterised by a moderate increase in velocity followed by a slight decrease. The velocity of inner drops was increased due to dissipation of the vortex flow, while the subsequent decrease in velocity was due to the break-up of the next outer drop after encapsulation of all inner drops.

The middle phase jet has the minimum velocity just after the pinch-off of each outer drop due to recoiling of the jet interface as a result of high capillary pressure in the thread connecting the detaching drop to the remaining. This decrease in velocity of the middle phase jet in the collection tube can be observed in the video

recordings of double emulsion drop formation (Movies 1–3 in the Supplementary material S1). In order to identify the additional factors that can possibly affect the break-up mechanism, the flow field during the outer drop pinch-off was visualised with polystyrene tracer beads (Fig. 3).

The effect of Brownian motion can significantly affect the instantaneous velocity field [27]. In the current study, however, due to the large size of tracer particles (d_t = 2 μm), high characteristic velocity ($V_3 \sim 7.4$ mm/s), and high dynamic viscosity of the outer fluid in which the tracer particles were suspended, the Brownian motion effect was negligible. The relative error due to Brownian motion, ε_B, can be estimated from [28]:

$$\varepsilon_B = \frac{1}{V_3}\sqrt{\frac{2D_{dif}}{\Delta t}} \quad (1)$$

where Δt is the time interval between two successive frames (0.5 ms), and D_{dif} (m^2/s) is the diffusion coefficient of the tracer particles given by the Stokes-Einstein equation:

$$D_{dif} = \frac{\kappa T}{3\pi\mu_3 d_t} \quad (2)$$

where T is the absolute temperature, and κ is Boltzmann's constant. The ε_B value calculated from Eq. (1) was 0.07% implying the negligible effect of Brownian motion on the normalised velocity profiles in Fig. 3. In Fig. 3a–c, it was found that the primary neck narrowing was accompanied by the formation of vortex flow tending to push backward and forward the outer interface at the upstream and downstream end of the neck, respectively, which eventually resulted in the thread break-up (Fig. 3d). Once the thread pinched off, the detached drop accelerated downstream, followed by rapid retreat of the elongated middle phase filament attached to the primary outer drop (shown in the red dashed rectangle in Fig. 3d). It is driven by the imbalance in capillary pressure across the interface and the presence of vortex flow.

On the other hand, a backflow upstream of the neck exerted a backward force that caused a deceleration of the middle phase jet and low velocity in the region shown by the black dotted box in Fig. 3d. The presence of vortex flow during necking of the middle phase jet that facilitated the jet break-up was observed numerically by Nabavi et al. [24].

3.2. Predicting number of inner drops

In this section, the effect of capillary numbers of inner, middle and outer fluids on the size and number of inner drops will be investigated by mapping flow patterns and identifying regions where monodisperse drops with a stable number of inner drops (N_d) can be formed.

Figs. 4a.1–c.1 are phase diagrams plotting N_D as a function of Ca_1, Ca_2, and Ca_3 for the fluids indicated in Table 1. The capillary numbers were varied by changing the flow rates of the inner, middle and outer fluids. The experimental data used to construct these diagrams are shown in Fig. s.2. The hatched blue, green, and light pink areas are the transitional regions where N_d varied with time within the limits specified in the legend. For example, the hatched green area represents the region where the number of inner drops varied between 2 and 4. On the other hand, the solid black, cyan, yellow, and red areas represent the regions where N_d was stable over longer time periods, and equal to one, two, four and six, respectively. The formation of uniform drops occurred when Ca_1 was greater than Ca_2 or Ca_3 by 2–4 orders of magnitude. The maximum stable N_D value of 6 was achieved at $Ca_3 = 4.6 \times 10^{-3}$. Monodispersed multi-core drops were created within the Ca_2 range of $(1.5–4.8) \times 10^{-4}$. For $Ca_2 < 1.5 \times 10^{-4}$, N_d was either 1 or varied uncontrollably between 1 and 2. For $Ca_2 > 4.8 \times 10^{-4}$, a continuous jet of middle phase encapsulating numerous uniform inner drops was formed (Fig. 4f).

Lower Ca_3 and higher Ca_2 and Ca_1 values favoured formation of drops with larger numbers of inner drops; e.g., at $Ca_1 = 0.42$ and $Ca_2 = 2.9 \times 10^{-4}$, a decrease in Ca_3 from 6.9×10^{-3} to 4.6×10^{-3} to 3.1×10^{-3} caused an increase in N_d from 1 to 2 to 4, respectively (Fig. s.3). A decrease in Ca_3 reduced the shear and pressure forces on the outer interface exerted by the outermost fluid, which caused the jet widening in the collection capillary. The increased jet-to-orifice diameter ratio, D_j/D_{orif} is slowing down the rate of growth of perturbations on the outer interface due to its proximity to the wall [5,29], increasing the jet break-up lengths and allowing more inner drops to be encapsulated. However, Ca_3 should be large enough for the outer fluid to be able to draw the middle phase through the orifice. For $Ca_3 < 3.1 \times 10^{-3}$, the outer fluid was not able to focus the compound jet into the collection tube, which resulted in the leakage of the inner fluid into the outer phase (Fig. 4d).

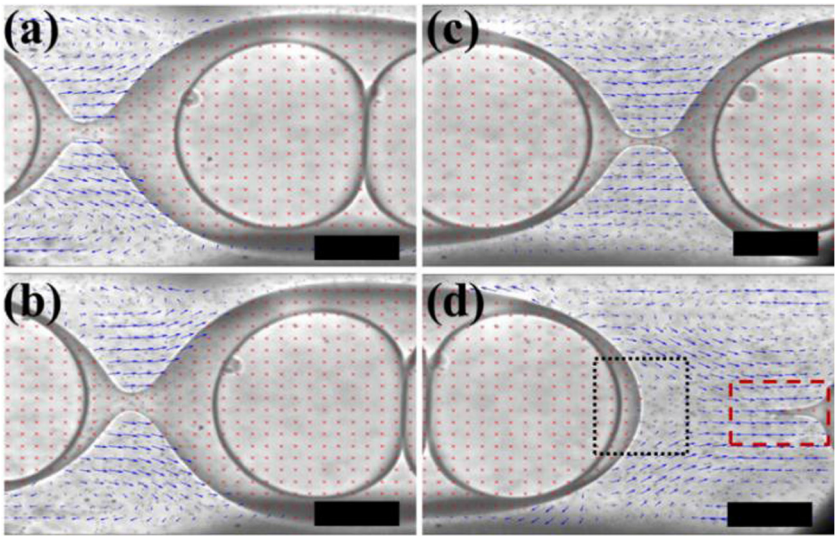

Fig. 3. Flow field visualisation of the jet pinch-off using μ-PIV. The outer drop consists of two inner drops. The dimensionless time is: (a) τ_0; (b) τ_0 + 26; (c) τ_0 + 186; (d) τ_0 + 348. All scale bars are 100 μm.

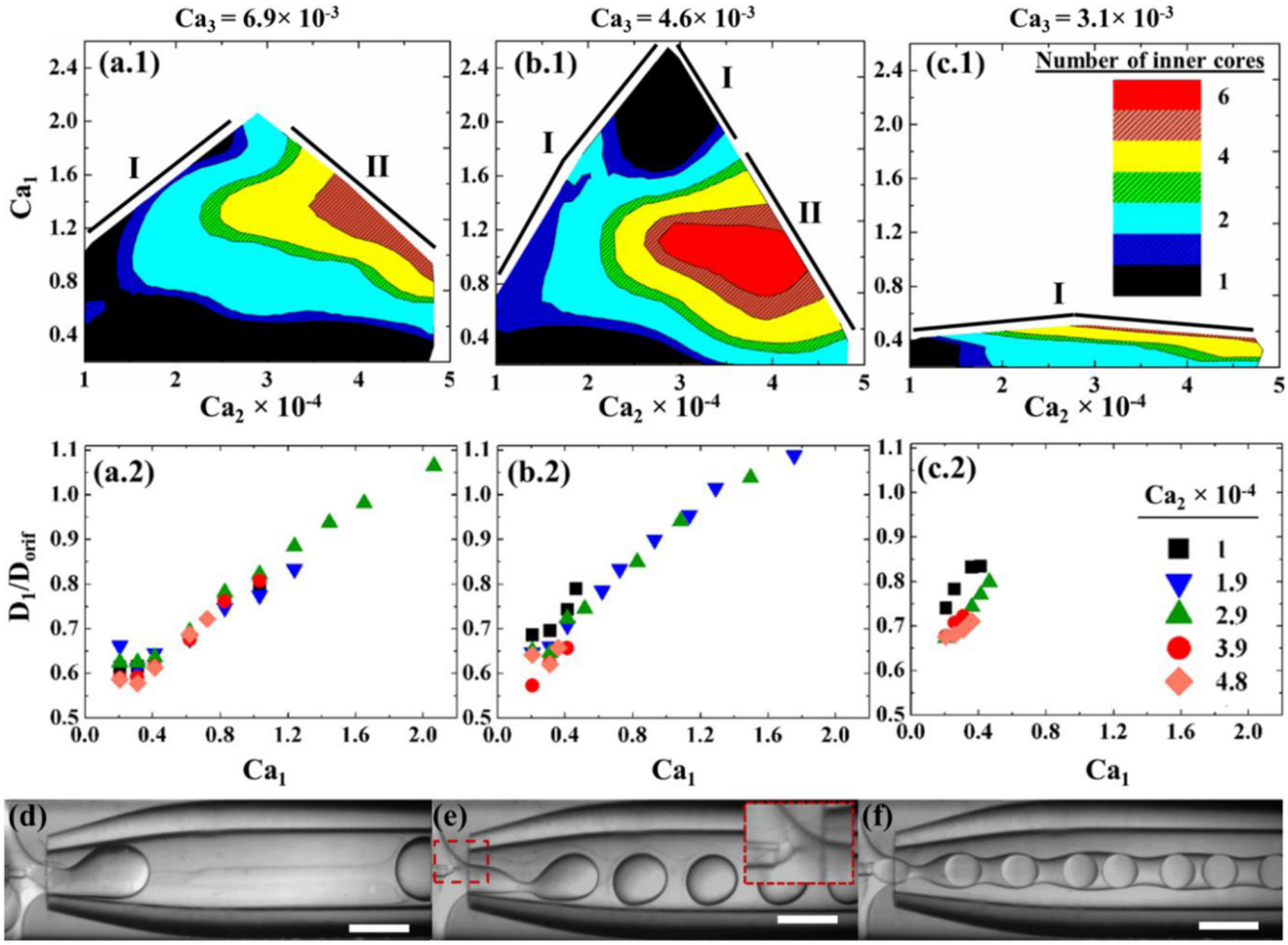

Fig. 4. The number of inner drops (a.1–c.1) and the diameters of inner drops (a.2–c.2) at: (a) $Ca_3 = 6.9 \times 10^{-3}$; (b) $Ca_3 = 4.6 \times 10^{-3}$; (c) $Ca_3 = 3.1 \times 10^{-3}$. (d–f) Unsuccessful production of double emulsion drops at: (d) $Q_1 = 0.2$ mL/h ($Ca_1 = 0.1$), $Q_2 = 0.4$ mL/h ($Ca_2 = 1 \times 10^{-4}$), $Q_3 = 3$ mL/h ($Ca_3 = 2.3 \times 10^{-3}$); (e) $Q_1 = 0.9$ mL/h ($Ca_1 = 0.5$), $Q_2 = 2$ mL/h ($Ca_2 = 4.8 \times 10^{-4}$), $Q_3 = 4$ mL/h ($Ca_3 = 3.1 \times 10^{-3}$); (f) $Q_1 = 2.2$ mL/h ($Ca_1 = 1.1$), $Q_2 = 2$ mL/h ($Ca_2 = 4.8 \times 10^{-4}$), $Q_3 = 9$ mL/h ($Ca_3 = 6.9 \times 10^{-3}$). The constant parameters: $D_{orif} = 327$ μm and $D_N = 50$ μm. The scale bars are 400 μm and the fluid properties are listed in Table 1.

When Ca_1 and Ca_3 were kept constant, N_d increased with increasing Ca_2 (Fig. 4a.1–c.1), because outer drops grew to a larger size before breaking off and thus, more inner drops could be encapsulated [23]. In addition, higher Ca_2 values at constant Ca_1 led to smaller inner drops, due to higher shear force acting on the inner fluid (Fig. 4a.2–c.2). A decrease in D_1 led to an increase in the frequency of inner drop formation, which resulted in higher N_d.

Increasing Ca_1 above a certain threshold value at constant Ca_2 and Ca_3 resulted in unsuccessful generation of multiple emulsion drops; two possible scenarios are shown in Fig. 4e and f. The flow behaviour shown in Fig. 4e was observed above the boundary line I in the phase diagram, which means at low Ca_3 and/or low Ca_2 values. In that case, due to small Q_2/Q_1 ratio, the inner fluid leaked into the outer fluid (the red dashed box in Fig. 4e). The flow behaviour shown in Fig. 4f and Movie 4 (in Supplementary material S1) occurred above the boundary line II when the volume fraction of the middle phase was higher than that of the inner phase. In that case, a high frequency of generation of inner drops suppressed perturbations of the outer interface, which led to the formation of a continuous middle phase jet loaded with numerous inner drops. This drop generation regime can be used for fabrication of hybrid microfibers [30,31].

Regarding the effect of Ca_1 on N_d, two different behaviours were observed. At $Ca_1 < 1$, the inertia of the inner fluid was small compared to viscous forces acting on the inner interface and N_d increased with increasing Ca_1. At $3 > Ca_1 > 1$, inertial forces domi-

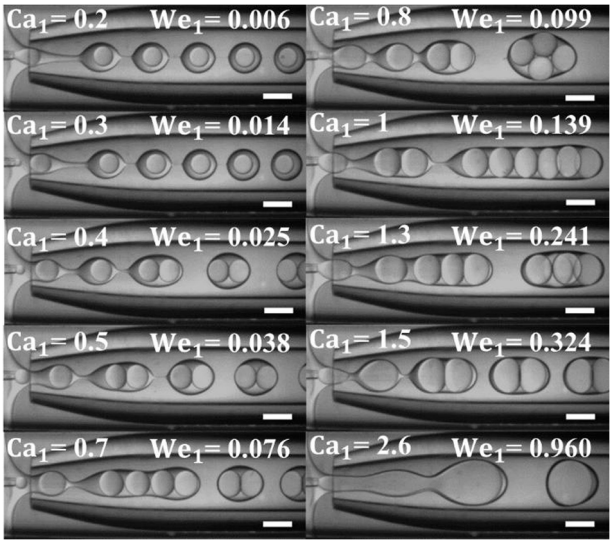

Fig. 5. The effect of the Capillary and Weber number of the inner phase, Ca_1 and We_1, on the drop formation behaviour at $Q_1 = 0.4$–5 mL/h. The constant parameters: $Q_2 = 1.2$ mL/h ($Ca_2 = 2.9 \times 10^{-4}$), $Q_3 = 6$ mL/h ($Ca_3 = 4.6 \times 10^{-3}$), $D_{orif} = 327$ μm, and $D_N = 50$ μm. The fluid properties are shown in Table 1 and the scale bars are 300 μm.

nated over viscous forces and N_d decreased with increasing Ca_1 due to an increase in the size of the inner drops (Fig. 5). It should be noted that D_1 increased with increasing Ca_1 over the entire range of Ca_1 investigated, although at high Ca_2 and Ca_3 values, D_1 was nearly constant at $Ca_1 < 0.4$ (Fig. 4a.2–b.2).

An empirical correlation was developed to predict D_1 as a function of Ca_1, Ca_2, Ca_3, and D_{orif}, based on experimental data obtained at different fluid flow rates:

$$\frac{D_1}{D_{orif}} = 0.2\frac{Ca_1^{0.23}}{Ca_2^{0.06}Ca_3^{0.23}} \quad (3)$$

As shown in Fig. 6, Eq. (3) was in good agreement with the experimental data. The frequency of generation of inner drops, f_1 and the Capillary number of inner fluid, Ca_1 can be expressed as:

$$f_1 = \frac{6}{\pi}\frac{Q_1}{D_1^3} \quad (4)$$

$$Ca_1 = \frac{4}{\pi D_N^2}\frac{\mu_1}{\sigma_{12}}Q_1 \quad (5)$$

Substituting Eqs. (4) and (5) into Eq. (3) one obtains:

$$f_1 = 187.5\frac{D_N^2}{D_{orif}^3}\frac{\sigma_{12}}{\mu_1}Ca_1^{0.31}Ca_2^{0.18}Ca_3^{0.69} \quad (6)$$

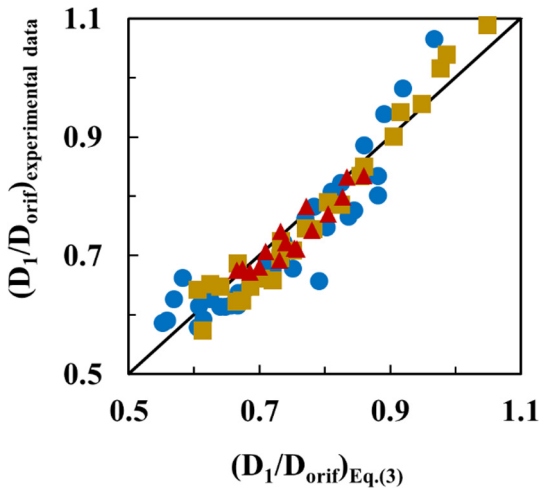

Fig. 6. A comparison between the experimental D_1 values and those calculated using Eq. (3) at Q_1 = 0.4–4 mL/h, Q_2 = 0.4–2 mL/h and: ● Q_3 = 9 mL/h; ■ Q_3 = 6 mL/h, ▲ Q_3 = 4 mL/h. The perfect match is shown by the diagonal line: $(D_1/D_{orif})_{exp} = (D_1/D_{orif})_{Eq.(3)}$.

According to Eq. (6), f_1 increases with increasing the capillary number of all fluids. In Fig. 5, an increase in Ca_1 from 0.2 to 2.6 led to an increase in f_1 by a factor of 2.2. The same trend with an increase in f_1 and D_1 as a result of increase in Q_1 was observed by numerical simulations [23]. An increase in N_d from 1 to 6 at Ca_1 = 0.2–1 can be attributed to an increase in f_1 which suppressed the growth of the outer interface perturbations. On the other hand, a decrease in N_d from 6 to 1 at $Ca_1 > 1$ can be attributed to the change in the formation regime of inner drops. For $Ca_1 < 1$, inner drops were formed in the dripping regime very near to the orifice. In addition, We_1 was relatively low (0.006–0.139), implying that the inertia of the inner fluid was negligible, and the drop size depended on the interplay between interfacial and viscous forces. At higher We_1 values (0.139–0.324), the inertia of the inner fluid was higher and the inner drops were formed in the transitional regime between dripping and widening jetting. As a result, the inner drops pinched off further downstream, although they were still highly uniform, with a coefficient of variation of their sizes of less than 2%. A transition from dripping to widening jetting occurred at $We_1 \approx 0.60$ [23]. At We_1 = 0.96, both inner and outer drops were formed in the widening jetting mode (Fig. 5), characterised by much larger drops than in the dripping mode [23,32]. A comprehensive parametric study of the effects of fluid flow rates, fluid properties, and device geometry on the size of inner and outer drops in single-step microfluidic emulsification can be found in our previous work [23].

3.3. Production of polymeric capsules from stable and unstable inner drops

In this section, additional level of control over the size and internal structure of double emulsion drops has been achieved by controlled coalescence of inner drops. First, large monodispersed dual-core double emulsion drops were produced in dripping-to-widening jetting transitional regime by decreasing the amount of oil-soluble surfactant in the middle phase. The inner drops then coalesced within the outer drops to form monodispersed core/shell drops with thin shells. The core/shell drops formed in the dripping-to-widening jetting transitional regime are larger than the core/shell drops generated in dripping mode and can be produced at higher rates, which can be highly beneficial. The inner phase was 15 wt% aqueous solution of K_2CO_3 with trace amounts of the pH indicator m-cresol purple. The middle phase was SEMISCOSIL 949 UV A/B, a UV curable silicone adhesive, containing 0.5–2 wt% of DC 749 surfactant. The outer phase was an aqueous solution containing 70 wt% of glycerol and 1 wt% of PF-127. After generation of dual-core double emulsion drops, the middle phase was polymerised "on-the-fly" using a UV-A light source (250 W Hoenle UVAHAND 250 Mobile UV lamp). The minimum energy density and UV light irradiance needed for successful photopolymerisation

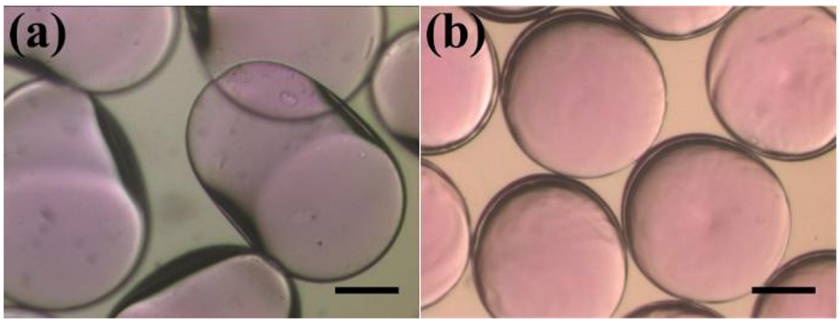

Fig. 7. (a) Non-spherical silicone rubber capsules with two cores made from dual-core drops using 2 wt% DC 749 in the middle phase; (b) Spherical single-core silicone rubber capsules produced by coalescence of two inner drops in the presence of 0.5 wt% DC 749 in the middle phase. The diameter of the capsules is 548 μm and the average shell thickness is 14 μm. The core liquid is 15 wt% aqueous solution of K_2CO_3 and the scale bars are 200 μm.

were 2 J·cm^{-2} and 13.8 mW·cm^{-2}, respectively. The morphology of the polymerised microcapsules depended on the stability of the inner drops during curing in the collection vial, which has been manipulated by changing the concentration of DC 749 surfactant in the middle phase.

When the surfactant concentration in the middle phase was 2 wt%, the inner drops were stable and the capsules made from such drops were non-spherical with two internal cavities (Fig. 7a). When the surfactant concentration in the middle phase was 0.5 wt%, the inner drops coalesced within the middle phase after generation of dual-core drops, but before shell curing. Therefore, destabilizing inner drops deliberately through insufficient amount of lipophilic surfactant in the middle phase is a promising approach for fabrication of relatively large single-compartment microcapsules with thin shells (Figs. 7b).

These large single-compartment silicon rubber capsules with encapsulated CO_2 absorbent are highly desirable for CO_2 capture in fluidised and packed bed systems due to their large gas/liquid interfacial area per unit volume (1.1×10^4 m^2/m^3 for the capsules in Fig. 7b as compared to 220–450 m^2/m^3 for typical structured packing). Also, silicon rubber has a high permeability to CO_2 of 323×10^{-9} cm^3·cm/(s·cm^2·cmHg) [25,26]. Small capsules suffer from poor fluidising properties, due to strong particle–particle adhesion, and can cause large pressure drops in packed bed systems. Therefore, microfluidic encapsulation of CO_2 solvents within gas-permeable polymer shells in dripping-to-widening jetting drop formation regime could be a promising tool to fabricate large capsules with a high capture capacity of typical liquid CO_2 solvents, which are suitable for use in fluidised and packed bed reactors.

4. Conclusions

The single-step formation of double emulsion drops with controlled number of inner cores in three phase glass capillary devices has been investigated using high-speed imaging combined with a micro-PIV system. Phase diagrams have been constructed based on the capillary numbers of the inner, middle and outer fluid to map out the regions where monodispersed double emulsion drops with specified number of inner drops can be generated. The pinch-off process of multi-core double emulsion was caused by a combination of high capillary pressure in the neck accompanied by the presence of a vortex flow. The formation of outer drops with multiple inner drops was achieved by decreasing the capillary number of the outer phase and increasing the capillary number of the middle phase. A stable continuous jet of middle phase loaded with uniform inner drops was formed at high capillary numbers of the middle phase, which could be exploited for fabrication of hybrid microfibres. At the capillary number of the inner fluid between 0.2 and 1, the inner drops were formed in the dripping regime and any increase in Ca_1 led to an increase in the number of inner drops. At Ca_1 = 1–2, double emulsion was formed in the dripping-to-widening jetting transitional mode and any increase in Ca_1 within this range resulted in the smaller number of inner drops. The maximum number of stable inner drops that could be formed within monodispersed outer drops was six.

The multiple emulsion drops consisting of two inner drops were used as templates to produce polymeric microcapsules using "on-the-fly" photopolymerisation. The capsule morphology was controlled by manipulating the stability of the inner drops through adjusting the concentration of the lipophilic surfactant in the middle phase. Non-spherical two-compartment capsules were synthetised at the surfactant concentration of 2 wt% due to high stability of the inner drops. A reduction in the surfactant concentration to 0.5 wt% led to destabilization and coalescence of inner drops and formation of large uniform single-compartment capsules. Multi-core double emulsion drops with unstable cores can be used as an alternative to millifluidic systems for fabrication of large core/shell microcapsules. Large capsules with gas-permeable shell and a gas absorbent in the core are highly desirable for gas absorption processes in packed bed absorption columns due to high gas/liquid interfacial area per unit volume and low operating pressure drops.

Acknowledgment

The authors gratefully acknowledge the financial support for this work from the UK Engineering and Physical Sciences Research Council (EPSRC) grant EP/HO29923/1. The authors also thank Mr. Ruslan Al-Dahle, Mr. Abdulkadir Hussein Sheik, and Dr. Hemaka Bandulasena for their help and support during the particle tracing measurement.

Appendix A. Supplementary data

Supplementary data associated with this article can be found, in the online version, at http://dx.doi.org/10.1016/j.cej.2017.04.008.

References

[1] C.X. Zhao, Multiphase flow microfluidics for the production of single or multiple emulsions for drug delivery, Adv. Drug Deliv. Rev. 65 (2013) 1420–1446.
[2] H. Chen, Y. Zhao, Y. Song, L. Jiang, One-step multicomponent encapsulation by compound-fluidic electrospray, J. Am. Chem. Soc. 130 (2008) 7800–7801.
[3] J. Lahann, Recent progress in nano-biotechnology: compartmentalized micro- and nanoparticles via electrohydrodynamic co-jetting, Small 7 (2011) 1149–1156.
[4] W. Zhang, S. Zhao, W. Rao, J. Snyder, J.K. Choi, J. Wang, I.A. Khan, N.B. Saleh, P.J. Mohler, J. Yu, T.J. Hund, C. Tang, X. He, A novel core-shell microcapsule for encapsulation and 3D culture of embryonic stem cells, J. Mater. Chem. B 2013 (2013) 1002–1009.
[5] S.H. Kim, D.A. Weitz, One-step emulsification of multiple concentric shells with capillary microfluidic devices, Angew. Chem. Int. Ed. Engl. 123 (2011) 8890–8893.
[6] D. Lee, D.A. Weitz, Nonspherical colloidosomes with multiple compartments from double emulsions, Small 5 (2009) 1932–1935.
[7] F. Gao, Z.G. Su, P. Wang, G.H. Ma, Double emulsion templated microcapsules with single hollow cavities and thickness-controllable shells, Langmuir 25 (2009) 3832–3838.
[8] T. Nisisako, S. Okushima, T. Torii, Controlled formulation of monodisperse double emulsions in a multiple-phase microfluidic system, Soft Matter 1 (2005) 23–27.
[9] G.T. Vladisavljević, R. Al Nuumani, S.A. Nabavi, Microfluidic production of multiple emulsions, Micromachines 8 (2017) 75.
[10] L. Chu, A.S. Utada, R.K. Shah, J. Kim, D.A. Weitz, Controllable monodisperse multiple emulsions, Angew. Chem. Int. Ed. Engl. 46 (2007) 8970–8974.
[11] S.H. Kim, H. Hwang, C.H. Lim, J.W. Shim, S.M. Yang, Packing of emulsion droplets: structural and functional motifs for multi-cored microcapsules, Adv. Funct. Mater. 21 (2011) 1608–1615.
[12] J. Fidalgo, Â. Dias, A.M. Mendes, F.D. Magalhães, Production of monodisperse multivesiculated polyester particles with a T-junction microfluidic device, Chem. Eng. J. 233 (2013) 323–330.
[13] S. Okushima, T. Nisisako, T. Torii, T. Higuchi, Controlled production of monodisperse double emulsions by two-step droplet breakup in microfluidic devices, Langmuir 20 (2004) 9905–9908.
[14] T. Si, C. Yin, P. Gao, G. Li, H. Ding, X. He, B. Xie, R.X. Xu, Steady cone-jet mode in compound-fluidic electro-flow focusing for fabricating multicompartment microcapsules, Appl. Phys. Lett. 108 (2016) 021601–021604.
[15] W. Wang, R. Xie, X.J. Ju, T. Luo, L. Liu, D.A. Weitz, L.Y. Chu, Controllable microfluidic production of multicomponent multiple emulsions, Lab Chip 11 (2011) 1587–1592.
[16] A. Perro, C. Nicolet, J. Angly, S. Lecommandoux, J.F. Le Meins, A. Colin, Mastering a double emulsion in a simple co-flow microfluidic to generate complex polymersomes, Langmuir 27 (2011) 9034–9042.
[17] N.N. Deng, Z.J. Meng, R. Xie, X.J. Ju, C.L. Mou, W. Wang, L.Y. Chu, Simple and cheap microfluidic devices for the preparation of monodisperse emulsions, Lab Chip 11 (2011) 3963–3969.
[18] N.N. Deng, W. Wang, X.J. Ju, R. Xie, D.A. Weitz, L.Y. Chu, Wetting-induced formation of controllable monodisperse multiple emulsions in microfluidics, Lab Chip 13 (2013) 4047–4052.
[19] S.S. Lee, A. Abbaspourrad, S.H. Kim, Nonspherical double emulsions with multiple distinct cores enveloped by ultrathin shells, ACS Appl. Mater. Interfaces 6 (2014) 1294–1300.

[20] H.C. Shum, Y.J. Zhao, S.H. Kim, D.A. Weitz, Multicompartment polymersomes from double emulsions, Angew. Chem. Int. Ed. 50 (2011) 1648–1651.
[21] A.S. Utada, E. Lorenceau, D.R. Link, P.D. Kaplan, H.A. Stone, D.A. Weitz, Monodisperse double emulsions generated from a microcapillary device, Science 308 (2005) 537–541.
[22] A.R. Abate, J. Thiele, D.A. Weitz, One-step formation of multiple emulsions in microfluidics, Lab Chip 11 (2011) 253–258.
[23] S.A. Nabavi, G.T. Vladisavljević, S. Gu, E.E. Ekanem, Double emulsion production in glass capillary microfluidic device: parametric investigation of droplet generation behaviour, Chem. Eng. Sci. 130 (2015) 183–196.
[24] S.A. Nabavi, S. Gu, G.T. Vladisavljevi, E.E. Ekanem, Dynamics of double emulsion break-up in three phase glass capillary microfluidic devices, J. Colloid Interface Sci. 450 (2015) 279–287.
[25] S.A. Nabavi, G.T. Vladisavljevic, S. Gu, V. Manovic, Semipermeable elastic microcapsules for gas capture and sensing, Langmuir 32 (2016) 9826–9835.
[26] J.J. Vericella, S.E. Baker, J.K. Stolaroff, E.B. Duoss, J.O. Hardin, J. Lewicki, E. Glogowski, W.C. Floyd, C.A. Valdez, W.L. Smith, J.H. Satcher, W.L. Bourcier, C.M. Spadaccini, J.A. Lewis, R.D. Aines, Encapsulated liquid sorbents for carbon dioxide capture, Nat. Commun. 6 (2015) 6124–6130.
[27] K. Shinohara, Y. Sugii, A. Aota, A. Hibara, M. Tokeshi, T. Kitamori, K. Okamoto, High-speed micro-PIV measurements of transient flow in microfluidic devices, Meas. Sci. Technol. 15 (2004) 1965–1970.
[28] J.G. Santiago, S.T. Wereley, C.D. Meinhart, D.J. Beebe, R.J. Adrian, A particle image velocimetry system for microfluidics, Exp. Fluids 25 (1998) 316–319.
[29] P. Guillot, A. Colin, A.S. Utada, A. Ajdari, Stability of a jet in confined pressure-driven biphasic flows at low Reynolds numbers, Phys. Rev. Lett. 99 (2007) 104502–104505.
[30] A.S. Chaurasia, F. Jahanzad, S. Sajjadi, Flexible microfluidic fabrication of oil-encapsulated alginate microfibers, Chem. Eng. J. 308 (2017) 1090–1097.
[31] A.S. Chaurasia, S. Sajjadi, Flexible asymmetric encapsulation for dehydration-responsive hybrid microfibers, Small 12 (2016) 4146–4155.
[32] Y. Chen, L. Wu, C. Zhang, Emulsion droplet formation in coflowing liquid streams, Phys. Rev. E 87 (2013) 013002–013009.